PERGAMON

International Journal of Heat and Mass Transfer 42 (1999) 357–372

International Journal of HEAT and MASS TRANSFER

Unsteady mixed convection boundary-layer flow on a vertical surface in a porous medium

S.D. Harris[a], D.B. Ingham[a,*], I. Pop[b]

[a] *Department of Applied Mathematical Studies, University of Leeds, Leeds LS2 9JT, West Yorkshire, U.K.*
[b] *Faculty of Mathematics, University of Cluj, R-3400 CLUJ, CP 253, Romania*

Received 11 December 1997

Abstract

An analysis is made of the unsteady mixed convection from a vertical flat plate embedded in a fluid-saturated porous medium. For time $t < 0$ a uniform free stream velocity U exists parallel to the plate surface and the temperature T_∞ throughout the porous medium is uniform. Then at time $t = 0$ the temperature on the surface is instantaneously changed from the ambient fluid temperature T_∞ to T_w. At small times the transport effects are confined within a narrow layer adjacent to the plate. As this inner boundary layer evolves, a steady boundary layer is approached but far from the plate the ambient conditions remain. A complete analysis is made of the governing equations at $t = 0$, the steady state at large times and a series solution valid at small times is derived. A numerical solution of the full boundary-layer equations is then obtained for the whole transient from $t = 0$ to the steady state. Results are presented to illustrate the occurrence of transients when the buoyancy parameter is positive (buoyancy and free stream forces in the same direction) and negative (buoyancy and free stream forces in opposing directions). The uniqueness of this problem lies in the fact that we have been able to match significantly different profiles at the time when the forward integration approach breaks down and the solution at large times and establish a smooth evolution around the transition time.

Nomenclature

f non-dimensional, reduced streamfunction $=(2\alpha Ux)^{-1/2}\xi^{-1/2}\psi$
$\mathscr{F}$ initial unsteady solution for f at $\xi = 0$, $\tau = 0$
g magnitude of the acceleration due to gravity
$G_2, \ldots, G_N$ system of $(N-1)$ nonlinear algebraic equations
Gr Grashof number $= g\beta K(T_w - T_\infty)x/\nu^2$
$\mathscr{G}$ steady-state solution for f at $\xi = 1$, $\tau = \infty$
h step length in η-direction for $0 \leqslant \xi \leqslant \xi^*$
$\tilde{h}$ step length in η-direction for $\xi^* \leqslant \xi \leqslant 1$
$\mathscr{H}$ small ξ or τ solution for f
k local heat transfer coefficient
$\tilde{k}$ non-dimensional ξ increment for $\xi^* \leqslant \xi \leqslant 1$
J Jacobian matrix
K permeability of the porous medium
L lower-triangular matrix
m number of grid spacings in the ξ-direction for $\xi^* \leqslant \xi \leqslant 1$
n number of grid spacings in the η-direction for $\xi^* \leqslant \xi \leqslant 1$
N number of grid spacings in the η-direction for $0 \leqslant \xi \leqslant \xi^*$
Nu Nusselt number $= xq_w/k(T_w - T_\infty)$
p, q variable coefficients in the governing equation for $\xi^* \leqslant \xi \leqslant 1$
Pe Péclet number $= Ux/\alpha$
q_w heat flux from the surface
Ra Rayleigh number $= g\beta K(T_w - T_\infty)x/\alpha\nu$
Re Reynolds number $= Ux/\nu$
S sum of numerical solutions for Φ over consecutive ξ-steps
t time
T fluid temperature
T_w constant surface temperature, $\xi \geqslant 0$
T_∞ ambient fluid temperature
u, v seepage velocity components along x- and y-axes, respectively

* Corresponding author

0017–9310/98/$—see front matter
PII: S0017–9310(98)00209–9

U uniform free stream velocity
$\mathbf{U}$ upper-triangular matrix
x, y Cartesian coordinates along the surface and normal to it, respectively.

Greek symbols
α effective thermal diffusivity
β volumetric coefficient of thermal expansion
$\varepsilon_1, \varepsilon_2, \varepsilon_3$ tolerances in the numerical schemes
η non-dimensional transformed variable $= y[U/2\alpha x]^{1/2}\xi^{-1/2}$
η_∞ η value regarded as being equivalent to $\eta = \infty$
θ non-dimensional temperature function $= (T-T_\infty)/(T_w-T_\infty)$
Θ, Ω expressions defined in equation (57)
λ buoyancy parameter $= g\beta K(T_w-T_\infty)/Uv$
λ_0 minimum buoyancy parameter for which solutions exist at $\xi = 1$
v kinematic viscosity
ξ non-dimensional transformed variable $= 1-e^{-\tau}$
$\Delta\xi$ non-dimensional ξ increment for $0 \leqslant \xi \leqslant \xi^*$
$\Delta\xi_0$ initial non-dimensional ξ increment at $\xi = 0$
σ ratio of composite material heat capacity to convective fluid heat capacity
τ non-dimensional time $= Ut/\sigma x$
Φ non-dimensional velocity function $\partial f/\partial\eta$
$\check{\Phi}$ expression defined in equation (65)
χ_1, χ_2, Λ expressions defined in equation (57)
ψ streamfunction
ω relaxation parameter.

Subscripts
i, j evaluated at the ith and jth nodal points in the η- and τ-directions, respectively.

Superscripts
$-$ variables used in the $\xi = 1, \lambda \to \infty$ solution
$*$ point where the forward integration approach of Section 5.1 breaks down
$\hat{}$ point where the forward integration approach is predicted to break down
(0) evaluated using an approximate solution.

1. Introduction

Convective flow through porous media is a branch of research undergoing rapid growth in fluid mechanics and heat transfer. This is quite natural because of its important applications in environmental, geophysical and energy related engineering problems. Prominent applications are the utilization of geothermal energy, the control of pollutant spread in groundwater, the design of nuclear reactors, compact heat exchangers, solar power collectors, heat transfer associated with the deep storage of nuclear waste and high performance insulations for buildings, as well as the heat transfer from stored agricultural products that release energy as a result of metabolism of the products. The growing volume of work devoted to this area is amply documented in the recent excellent reviews by Nield and Bejan [1], Kaviany [2], Nakayama [3] and Ingham and Pop [4]. There is still a great deal of interest in this area, both from a theoretical and practical point of view. On the practical side, there is interest in a new generation of engineering problems connected with the topical issues of thermal insulation engineering, and on the theoretical side there remains a continuous need for a comprehensive theoretical framework which covers the field in much the same way as the solutions of the Navier–Stokes and energy conservation equations cover thermal convection in viscous (non-porous) fluids.

Most of the recent research on convective flow in porous media have been directed on the problems of steady free and mixed convection flows over heated bodies embedded in fluid-saturated porous media. Unsteady convective boundary-layer flow problems, on the other hand, have not, so far, received as much attention. Perhaps, the first study on the unsteady boundary-layer flow on a flat plate was made by Johnson and Cheng [5] who found similarity solutions for certain variations of the wall temperature. The more common cases, in general, involve transient convection which is non-similar and hence more complicated mathematically. Subsequently, some studies were performed to analyze the unsteady free convection from vertical and horizontal flat plates in Darcian or non-Darcian porous media. Ingham et al. [6, 7] exploited asymptotic expansions to study the problem of transient free convection from suddenly cooled vertical and horizontal isothermal flat plates embedded in a porous medium, while Pop and Cheng [8] and Cheng and Pop [9] used the integral method to investigate the transient free convection boundary layers from suddenly heated isothermal horizontal and vertical surfaces in porous media. Further, Ingham and Brown [10] and Merkin and Zhang [11] allowed the wall temperature, or wall heat flux, to vary according to a power function of the distance from the leading edge. More recently, Harris et al. [12–14] have produced very detailed studies of the problem of transient free convection from a vertical isothermal flat plate immersed in a fluid-saturated porous medium when the temperature of the plate, or heat flux, is suddenly changed. The interested reader can find an excellent collection of papers on unsteady convective flow problems over heated bodies embedded in a fluid-saturated porous medium in the review papers by Pop et al. and Bradean et al., which are in the book by Ingham and Pop [4].

A review of the literature shows that very little research has been reported on unsteady mixed convection flow in porous media. Based on the review above, it is clear that the unsteady mixed convection along a vertical flat plate

has not so far been studied. However, this situation is important in cooling applications of electronic devices in which the heat generating rate is not a constant but time-varying. Therefore, the aim of the present paper is to investigate the boundary-layer development along a vertical isothermal semi-infinite flat plate when the temperature of the plate is suddenly raised at time $t = 0$ from that of the surrounding fluid. The governing Darcy and energy equations are transformed using semi-similar coordinates originated by Smith [15] and very recently extended to some forced convection heat transfer problems of viscous (non-porous) fluids by Bhattacharyya et al. [16] and Kumari and Nath [17]. This is the method of semi-similar solutions, in which the number of independent variables is reduced from three to two by an appropriate scaling. The scale of time has been selected in such a manner that the traditional infinite region is transformed to a finite region, which reduces the computational time considerably. A complete analysis is made of the transformed boundary-layer equations for a wide range of values of the buoyancy parameter λ. A closed form solution of these equations has been shown to exist at $t = 0$ (the initial unsteady flow), as $t \to \infty$ (the final steady flow) and for small times t. A very efficient step-by-step numerical solution of the full boundary-layer equations was then obtained for the whole transient regime when the buoyancy parameter λ is positive (assisting flow) and negative (opposing flow), respectively. The results are believed to be very consistent which, potentially, make them of importance to future theoretical studies of convective flow problems in porous media.

2. Governing equations

The initial situation is that of two-dimensional, uniform flow with constant velocity U vertically past a semi-infinite vertical flat plate which is embedded in a fluid-saturated porous medium. For times $t < 0$ the plate and the surrounding porous medium are at the uniform, constant temperature T_∞. At time $t = 0$ the temperature on the plate is suddenly changed to T_w and maintained at this value for $t > 0$. With the usual boundary-layer and Darcy–Boussinesq approximations [1], the governing equations for the transient response are

$$\frac{\partial u}{\partial x} + \frac{\partial v}{\partial y} = 0 \tag{1}$$

$$u = U + \frac{g\beta K}{v}(T - T_\infty) \tag{2}$$

$$\sigma\frac{\partial T}{\partial t} + u\frac{\partial T}{\partial x} + v\frac{\partial T}{\partial y} = \alpha\frac{\partial^2 T}{\partial y^2}. \tag{3}$$

The conditions

$$u(x, y, t) = U, \quad v(x, y, t) = 0, \quad T(x, y, t) = T_\infty \tag{4}$$

which are valid for $t < 0$ and $-\infty < x,\ y < \infty$, are replaced by the initial and boundary conditions

$$v(x, 0, t) = 0, \quad T(x, 0, t) = T_w$$
$$u(x, y, t) \to U, \quad T(x, y, t) \to T_\infty \quad \text{as } y \to \infty \tag{5}$$

for $t \geqslant 0$ and $0 \leqslant x < \infty$, in which the free stream velocity, U, and temperature, T_∞, are maintained at large distances away from the plate surface. Here $u(x, y, t)$ and $v(x, y, t)$ denote the seepage velocity components along the x- and y-directions, with x being measured along the surface starting at the leading edge and y measured normal to it, $T(x, y, t)$ is the fluid temperature, β is the coefficient of thermal expansion, K is the permeability of the porous medium, g is the acceleration due to gravity, v is the kinematic viscosity, σ is the heat capacity ratio and α is the effective thermal diffusivity of the fluid-saturated porous medium.

To solve equations (1)–(3) for $t \geqslant 0$, we introduce the non-dimensional, time dependent, reduced stream-function, f, and the temperature function, θ, which are defined as

$$\psi = (2\alpha Ux)^{1/2}\xi^{1/2}f(\xi, \eta), \quad \theta(\xi, \eta) = \frac{T - T_\infty}{T_w - T_\infty} \tag{6}$$

where

$$\tau = \frac{Ut}{\sigma x}, \quad \xi = 1 - e^{-\tau}, \quad \eta = y\left[\frac{U}{2\alpha x}\right]^{1/2}\xi^{-1/2} \tag{7}$$

$0 \leqslant \xi \leqslant 1$ and ψ is the streamfunction which is defined in the usual way, namely $u = \partial\psi/\partial y$ and $v = -\partial\psi/\partial x$. Expressions (6) and (7) correspond to the semi-similarity transformation originated by Smith [15] and presented in Bhattacharyya et al. [16].

Applying the transformation of variables (6) and (7) to the governing equations (2) and (3) leads to

$$\frac{\partial f}{\partial \eta} = 1 + \lambda\theta \tag{8}$$

and

$$\frac{\partial^2\theta}{\partial\eta^2} + [\xi + (1-\xi)\ln(1-\xi)]f\frac{\partial\theta}{\partial\eta} + (1-\xi)\eta\frac{\partial\theta}{\partial\eta} + 2\xi(1-\xi)\ln(1-\xi)\frac{\partial f}{\partial\xi}\frac{\partial\theta}{\partial\eta} = 2\xi(1-\xi)\left[1 + \ln(1-\xi)\frac{\partial f}{\partial\eta}\right]\frac{\partial\theta}{\partial\xi} \tag{9}$$

respectively, where

$$\lambda = \frac{g\beta K(T_w - T_\infty)}{Uv} = \frac{Ra}{Pe} = \frac{Gr}{Re} \tag{10}$$

is the buoyancy parameter and the Rayleigh number, Ra, Péclet number, Pe, Grashof number, Gr, and Reynolds number, Re, are defined explicitly as

$$Ra = \frac{g\beta K(T_w - T_\infty)x}{\alpha v}, \quad Pe = \frac{Ux}{\alpha},$$

$$Gr = \frac{g\beta K(T_w - T_\infty)x}{\nu^2}, \quad Re = \frac{Ux}{\nu}. \tag{11}$$

If $T_w > T_\infty$ the free stream and the buoyancy forces are in the same direction and therefore the buoyancy parameter, $\lambda > 0$ for aiding flows. Alternatively, if $T_w < T_\infty$ the free stream and the buoyancy forces are in the opposite direction and we have $\lambda < 0$ for opposing flows.

Equations (8) and (9) can be combined to produce a partial differential equation governing the evolution of the function f alone:

$$\frac{\partial^3 f}{\partial \eta^3} + [\xi + (1-\xi)\ln(1-\xi)] f \frac{\partial^2 f}{\partial \eta^2} + (1-\xi)\eta \frac{\partial^2 f}{\partial \eta^2} + 2\xi(1-\xi)\ln(1-\xi)\frac{\partial f}{\partial \xi}\frac{\partial^2 f}{\partial \eta^2} = 2\xi(1-\xi)\left[1 + \ln(1-\xi)\frac{\partial f}{\partial \eta}\right]\frac{\partial^2 f}{\partial \xi \partial \eta} \tag{12}$$

which must be solved over $0 \leqslant \xi \leqslant 1$ subject to the boundary conditions

$$f(\xi, 0) = 0, \quad \frac{\partial f}{\partial \eta}(\xi, 0) = 1 + \lambda, \quad \frac{\partial f}{\partial \eta}(\xi, \infty) = 1. \tag{13}$$

3. Initial unsteady and final steady solutions

The governing partial differential equation (12), and the associated boundary conditions (13), permit separate reductions to ordinary differential systems governing the profiles of the non-dimensional velocity and temperature functions in the initial unsteady state at $\xi = 0$ and the final steady state at large times given by $\xi = 1$. The system for the initial unsteady situation admits a closed form solution. The system for the large time steady state solution cannot be solved explicitly but is investigated both for λ large and λ in the vicinity of $\lambda = 0$. A complete analysis of the behaviour of the large time solution with variations in the buoyancy parameter λ is made in Section 6.1, where a numerical analysis of the governing ordinary differential system is carried out.

The Nusselt number, Nu, is defined in terms of the local heat transfer coefficient, k, and the heat flux from the surface, q_w, according to the relationship

$$Nu = \frac{xq_w}{k(T_w - T_\infty)} = -\frac{x}{T_w - T_\infty}\left(\frac{\partial T}{\partial y}\right)\bigg|_{y=0}. \tag{14}$$

Introducing the variables (6) and (7), we obtain the ratio

$$\frac{Nu}{Pe^{1/2}} = -(2\xi)^{-1/2}\frac{\partial \theta}{\partial \eta}(\xi, 0) = -\frac{1}{\lambda}(2\xi)^{-1/2}\frac{\partial^2 f}{\partial \eta^2}(\xi, 0) \tag{15}$$

using the Péclet number, Pe, defined in equation (11).

3.1. Initial unsteady solution at $\xi = 0$

The initial solution profile at $\xi = 0$, corresponding to $\tau = 0$, can be derived by applying the reduction $\xi = 0$ to the governing equation (12) and the associated boundary conditions (13). The function $f(0, \eta) = \mathscr{F}(\eta)$ then satisfies the ordinary differential system

$$\mathscr{F}''' + \eta\mathscr{F}'' = 0$$
$$\mathscr{F}(0) = 0, \quad \mathscr{F}'(0) = 1 + \lambda, \quad \mathscr{F}'(\infty) = 1 \tag{16}$$

where prime denotes differentiation with respect to η, which possesses the closed form solution

$$\mathscr{F}(\eta) = \eta + \lambda\left\{\eta\,\mathrm{erfc}\left(\frac{\eta}{\sqrt{2}}\right) + \sqrt{\frac{2}{\pi}}\left[1 - \mathrm{e}^{-\frac{\eta^2}{2}}\right]\right\}. \tag{17}$$

The non-dimensional velocity function profile at $\xi = 0$, given explicitly as

$$\mathscr{F}'(\eta) = 1 + \lambda\,\mathrm{erfc}\left(\frac{\eta}{\sqrt{2}}\right) \tag{18}$$

can then be used to obtain the non-dimensional skin friction coefficient at the plate surface in the initial unsteady state, namely

$$\mathscr{F}''(0) = -\lambda\sqrt{\frac{2}{\pi}}. \tag{19}$$

3.2. Steady solution at $\xi = 1$

The transport of energy at $\xi = 1$, corresponding to $\tau \to \infty$, is steady and hence $f(1, \eta) = \mathscr{G}(\eta)$, say, so that, from equation (12), $\mathscr{G}(\eta)$ satisfies the ordinary differential equation

$$\mathscr{G}''' + \mathscr{G}\mathscr{G}'' = 0 \tag{20}$$

which has to be solved subject to the boundary conditions (13) which reduce to

$$\mathscr{G}(0) = 0, \quad \mathscr{G}'(0) = 1 + \lambda, \quad \mathscr{G}'(\infty) = 1. \tag{21}$$

The configuration at $\xi = 1$, and therefore also the governing ordinary differential system equationss (20) and (21), can be derived as a special case of the general discussion of mixed convection about inclined surfaces presented in Cheng [18]. The behaviour of the solution of the systems (20) and (21) as the parameter λ is varied was also determined numerically by Merkin [19]. In the discussion that follows a brief analysis is made for $|\lambda| \ll 1$ and as $\lambda \to \infty$ and the variation in λ is interpreted in terms of the resultant flow situations using a numerical analysis in Section 6.1.

For $\lambda = 0$, equation (20) subject to the boundary conditions of equation (21) admits the closed form solution

$$\mathscr{G}(\eta) = \eta. \tag{22}$$

It is also possible to obtain an approximation to the solution of equation (20) for $\mathscr{G}(\eta)$ in the vicinity of $\lambda = 0$.

In this case we seek a power series solution of equation (20) of the form

$$\mathscr{G}(\eta) = \sum_{i=0}^{\infty} \mathscr{G}_i(\eta)\lambda^i \tag{23}$$

which is valid for $|\lambda| \ll 1$. Directly substituting the expansion (23) into the ordinary differential equation (20) and the boundary conditions (21) and equating coefficients of powers of λ up to second order leads to the three systems defining the first three functions $\mathscr{G}_0$, $\mathscr{G}_1$ and $\mathscr{G}_2$, namely

$$\mathscr{G}_0''' + \mathscr{G}_0\mathscr{G}_0'' = 0$$
$$\mathscr{G}_0(0) = 0, \quad \mathscr{G}_0'(0) = 1, \quad \mathscr{G}_0'(\infty) = 1 \tag{24}$$
$$\mathscr{G}_1''' + \mathscr{G}_0\mathscr{G}_1'' + \mathscr{G}_1\mathscr{G}_0'' = 0$$
$$\mathscr{G}_1(0) = 0, \quad \mathscr{G}_1'(0) = 1, \quad \mathscr{G}_1'(\infty) = 0 \tag{25}$$

and

$$\mathscr{G}_2''' + \mathscr{G}_0\mathscr{G}_2'' + \mathscr{G}_1\mathscr{G}_1'' + \mathscr{G}_2\mathscr{G}_0'' = 0$$
$$\mathscr{G}_2(0) = 0, \quad \mathscr{G}_2'(0) = 0, \quad \mathscr{G}_2'(\infty) = 0. \tag{26}$$

The solution $\mathscr{G}_0(\eta)$ of the system (24) is exactly the $\lambda = 0$ solution given in equation (22). The function

$$\mathscr{G}_1(\eta) = \eta\,\mathrm{erfc}\left(\frac{\eta}{\sqrt{2}}\right) + \sqrt{\frac{2}{\pi}}\left[1 - \mathrm{e}^{-\frac{\eta^2}{2}}\right] \tag{27}$$

where

$$\mathrm{erfc}(z) = \frac{2}{\sqrt{\pi}}\int_z^{\infty} \mathrm{e}^{-t^2}\,\mathrm{d}t$$

is the complementary error function, satisfying the system (25) and the function

$$\mathscr{G}_2(\eta) = \left[\sqrt{\frac{2}{\pi}}\left(\frac{3}{2}\mathrm{e}^{-\frac{\eta^2}{2}} + 1\right) - \frac{1}{2}\eta\,\mathrm{erfc}\left(\frac{\eta}{\sqrt{2}}\right) + \left(\frac{1}{2} + \frac{1}{\pi}\right)\eta\right]\mathrm{erfc}\left(\frac{\eta}{\sqrt{2}}\right) - \frac{2}{\sqrt{\pi}}\mathrm{erfc}(\eta) - \sqrt{\frac{2}{\pi}}\left[\left(\frac{1}{2} + \frac{1}{\pi}\right)\mathrm{e}^{-\frac{\eta^2}{2}} + 2 - \frac{1}{\pi} - \sqrt{2}\right] \tag{28}$$

satisfying the system (26) can then be used to obtain the first three terms in the velocity function

$$\begin{aligned}\mathscr{G}'(\eta) &= \mathscr{G}_0'(\eta) + \mathscr{G}_1'(\eta)\lambda + \mathscr{G}_2'(\eta)\lambda^2 + \mathbf{O}(\lambda^3)\\ &= 1 + \lambda\,\mathrm{erfc}\left(\frac{\eta}{\sqrt{2}}\right) + \lambda^2\left[\left(\frac{1}{2} + \frac{1}{\pi}\right)\mathrm{erfc}\left(\frac{\eta}{\sqrt{2}}\right) - \frac{1}{2}\mathrm{erfc}^2\left(\frac{\eta}{\sqrt{2}}\right) - \frac{1}{\sqrt{2\pi}}\eta\mathrm{e}^{-\frac{\eta^2}{2}}\,\mathrm{erfc}\left(\frac{\eta}{\sqrt{2}}\right) + \frac{1}{\pi}\mathrm{e}^{-\eta^2} - \frac{2}{\pi}\mathrm{e}^{-\frac{\eta^2}{2}}\right] + \mathbf{O}(\lambda^3)\end{aligned} \tag{29}$$

arising from the expansion (23) and valid for $|\lambda| \ll 1$. The derivative of expression (29) can be obtained and evaluated at $\eta = 0$ to give the non-dimensional skin friction coefficient at the plate surface

$$\mathscr{G}''(0) = -\sqrt{\frac{2}{\pi}}\lambda\left(1 + \frac{1}{\pi}\lambda\right) + \mathbf{O}(\lambda^3) \tag{30}$$

from which the ratio (15) for the final steady state at $\xi = 1$ has the explicit form

$$\frac{Nu}{Pe^{1/2}} = \frac{1}{\sqrt{\pi}}\left(1 + \frac{1}{\pi}\lambda\right) + \mathbf{O}(\lambda^2) \tag{31}$$

in the vicinity of $\lambda = 0$. In the reduction $\lambda = 0$, the ratio (31) becomes

$$\frac{Nu}{Pe^{1/2}} = \frac{1}{\sqrt{\pi}}$$

and describes the case of pure forced convection.

An approximation to the solution of systems (20) and (21) which is valid as $\lambda \to \infty$ can be achieved by first introducing the function $\bar{\mathscr{G}}(\bar{\eta})$, defined according to

$$\mathscr{G}(\eta) = \lambda^{1/2}\bar{\mathscr{G}}, \quad \bar{\eta} = \lambda^{1/2}\eta \tag{32}$$

which satisfies the following ordinary differential system:

$$\bar{\mathscr{G}}''' + \bar{\mathscr{G}}\bar{\mathscr{G}}'' = 0 \bar{\mathscr{G}}(0) = 0, \quad \bar{\mathscr{G}}'(0) = 1, \quad \bar{\mathscr{G}}'(\infty) = 0 \tag{33}$$

whose solution is independent of the parameter λ. The behaviour of the solution $\mathscr{G}(\eta)$ at large values of λ can then be approximated using the function

$$\mathscr{G}''(0) \sim \lambda^{3/2}\bar{\mathscr{G}}''(0) \tag{34}$$

from which the asymptotic value of the ratio (15), namely

$$\frac{Nu}{Pe^{1/2}} \sim -\frac{1}{\sqrt{2}}\lambda^{1/2}\bar{\mathscr{G}}''(0) \tag{35}$$

can be found once we have solved the system equation (33) to give the value $\bar{\mathscr{G}}''(0)$.

4. Small ξ and small time solutions

The function $f(\xi, \eta)$ satisfying the governing partial differential equation (12), subject to the boundary conditions (13), can be expanded as a polynomial series in positive powers of ξ. Thus we define an approximation to $f(\xi, \eta)$ which is valid in the region $\xi \ll 1$, equivalent to small values of the non-dimensional time $\tau \ll 1$, by the explicit expression

$$f(\xi, \eta) = \sum_{i=0}^{\infty} \mathscr{H}_i(\eta)\xi^i. \tag{36}$$

Substituting this polynomial series into equation (12) and equating to zero the coefficients of powers of ξ up to terms of $\mathbf{O}(\xi^3)$ leads to the following systems of ordinary differential equations for the functions $\mathscr{H}_1(\eta)$, $\mathscr{H}_2(\eta)$ and $\mathscr{H}_3(\eta)$:

$$\mathscr{H}_1''' + \eta\mathscr{H}_1'' - 2\mathscr{H}_1' = \eta\mathscr{H}_0'' \tag{37}$$

$$\mathscr{H}_2''' + \eta\mathscr{H}_2'' - 4\mathscr{H}_2' = \eta\mathscr{H}_1'' + 2\mathscr{H}_1\mathscr{H}_0'' - \tfrac{1}{2}\mathscr{H}_0\mathscr{H}_0'' - 2\mathscr{H}_1' - 2\mathscr{H}_0'\mathscr{H}_1' \quad (38)$$

$$\mathscr{H}_3''' + \eta\mathscr{H}_3'' - 6\mathscr{H}_3' = \eta\mathscr{H}_2'' + 2\mathscr{H}_1\mathscr{H}_1'' - \tfrac{1}{2}\mathscr{H}_0\mathscr{H}_1'' + 4\mathscr{H}_2\mathscr{H}_0'' - \tfrac{3}{2}\mathscr{H}_1\mathscr{H}_0'' - \tfrac{1}{6}\mathscr{H}_0\mathscr{H}_0'' - 4\mathscr{H}_2' - 4\mathscr{H}_0'\mathscr{H}_2' - 2(\mathscr{H}_1')^2 + \mathscr{H}_0'\mathscr{H}_1' \quad (39)$$

$$\mathscr{H}_i(0) = 0, \quad \mathscr{H}_i'(0) = 0, \quad \mathscr{H}_i'(\infty) = 0, \quad i = 1, 2, 3 \quad (40)$$

where the boundary conditions follow by extending the expansion (36) to the original boundary conditions (13). The function $\mathscr{H}_0(\eta)$ satisfies precisely equation (16), namely the system at $\xi = 0$, and is therefore given by equation (17). Closed form expressions for the functions $\mathscr{H}_1(\eta)$, $\mathscr{H}_2(\eta)$ and $\mathscr{H}_3(\eta)$ can be recovered by successively solving the systems (37)–(39), subject to the boundary conditions (40), to give

$$\mathscr{H}_1(\eta) = \frac{1}{4}\lambda\sqrt{\frac{2}{\pi}}\left(1 - \mathrm{e}^{-\frac{\eta^2}{2}}\right) \quad (41)$$

$$\mathscr{H}_2(\eta) = \frac{1}{96}\lambda\sqrt{\frac{2}{\pi}}\left(13 - (3\eta^2 + 13)\,\mathrm{e}^{-\frac{\eta^2}{2}}\right) \quad (42)$$

$$\mathscr{H}_3(\eta) = \frac{1}{384}\lambda\sqrt{\frac{2}{\pi}}\left(35 - (\eta^4 + 10\eta^2 + 35)\,\mathrm{e}^{-\frac{\eta^2}{2}}\right). \quad (43)$$

The resulting expression for the non-dimensional velocity function $\partial f/\partial\eta\ (\xi, \eta)$ at small values of ξ is given by

$$\frac{\partial f}{\partial\eta}(\xi, \eta) = 1 + \lambda\,\mathrm{erfc}\left(\frac{\eta}{\sqrt{2}}\right) + \frac{1}{384}\lambda\sqrt{\frac{2}{\pi}}[96\eta\xi + 4(3\eta^2 + 7)\eta\xi^2 + (\eta^4 + 6\eta^2 + 15)\eta\xi^3]\,\mathrm{e}^{-\frac{\eta^2}{2}} + \mathbf{O}(\xi^4). \quad (44)$$

Equation (8) then determines the small time evolution of the non-dimensional temperature function, θ, as

$$\theta = \mathrm{erfc}\left(\frac{\eta}{\sqrt{2}}\right) + \frac{1}{192}\sqrt{\frac{2}{\pi}}[48\eta\tau + 4(3\eta^2 - 5)\eta\tau^2 + 3(\eta^4 - 6\eta^2 + 3)\eta\tau^3]\,\mathrm{e}^{-\frac{\eta^2}{2}} + \mathbf{O}(\tau^4) \quad (45)$$

at small times τ, using the approximate polynomial relationship

$$\xi = \tau - \tfrac{1}{2}\tau^2 + \tfrac{1}{6}\tau^3 + \mathbf{O}(\tau^4) \quad (46)$$

between ξ and τ which follows from the definition (7).

The approximation to the non-dimensional skin friction coefficient at the plate surface

$$\frac{\partial^2 f}{\partial\eta^2}(\xi, 0) = \lambda\sqrt{\frac{2}{\pi}}\left(-1 + \frac{1}{4}\xi + \frac{7}{96}\xi^2 + \frac{5}{128}\xi^3\right) + \mathbf{O}(\xi^4) \quad (47)$$

derived from equation (44), can then be used to predict the behaviour of the ratio (15) for small values of ξ as

$$\frac{Nu}{Pe^{1/2}} = \frac{1}{\sqrt{\pi}}\left[\xi^{-1/2} - \frac{1}{4}\xi^{1/2} - \frac{7}{96}\xi^{3/2} - \frac{5}{128}\xi^{5/2}\right] + \mathbf{O}(\xi^{7/2}). \quad (48)$$

In terms of the non-dimensional time, τ, the initial evolution of the skin friction coefficient (47) and the ratio (48) can be expressed as

$$\left.\frac{\partial^2 f}{\partial\eta^2}\right|_{\eta=0} = \lambda\sqrt{\frac{2}{\pi}}\left(-1 + \frac{1}{4}\tau - \frac{5}{96}\tau^2 + \frac{1}{128}\tau^3\right) + \mathbf{O}(\tau^4) \quad (49)$$

and

$$\frac{Nu}{Pe^{1/2}} = \frac{1}{\sqrt{\pi}}\tau^{-1/2} + \mathbf{O}(\tau^{7/2}). \quad (50)$$

The initial evolutions of the ratio (50) and the non-dimensional temperature function θ, given in equation (45), are independent of λ to at least $\mathbf{O}(\tau^{7/2})$, but the steady state solutions given in Section 3.2 show that this is not the case as we approach $\xi = 1$.

5. Numerical techniques

Initially the transient effects due to the temperature difference between the free stream flow and the plate surface are confined to a region near to the surface and the situation can be approximated by the small ξ and small time solutions developed in Section 4. These effects continue to penetrate outwards and eventually evolve into a steady state, boundary-layer flow at $\xi = 1$, corresponding to $\tau \to \infty$. In order to match the small ξ, or τ, to the $\xi = 1$, or large time, solution we now develop a numerical solution of the full boundary-layer equations (1)–(3) in their non-dimensional form (12).

The governing partial differential equation (12) is parabolic and can be integrated numerically using a step-by-step method similar to that described by Merkin [20], provided that the term $[1 + \ln(1-\xi)\partial f/\partial\eta]$ in the coefficient of $\partial^2 f/\partial\xi\partial\eta$ remains positive throughout the η domain. This implicit finite-difference scheme enables the solution $\mathscr{F}(\eta)$ at $\xi = \tau = 0$ to proceed in ξ and gives a complete solution for $\xi \leqslant \xi^*$, which is equivalent to $\tau \leqslant \tau^*$. The value $\xi = \xi^*$ is the maximum ξ reached in the forward integration method, which may differ slightly from the precise value $\xi = \hat{\xi}$ satisfying the relationship

$$\ln(1 - \hat{\xi})\frac{\partial f}{\partial\eta}(\hat{\xi}, \eta_m) = -1. \quad (51)$$

The solution of equation (51) represents the first ξ at which the coefficient of $\partial^2 f/\partial\xi\partial\eta$ equals zero and thus the derivative $\partial f/\partial\eta$ must be evaluated at the position $\eta = \eta_m$

which maximizes this velocity function. For aiding flows, $\lambda > 0$, the velocity function takes its maximum value $(1+\lambda)$ at the plate surface, $\eta_m = 0$. For opposing flows, $\lambda < 0$, the magnitude of the velocity function reduces as we approach the plate surface so that the maximum value of $\partial f/\partial\eta = 1$ is achieved at $\eta_m = \infty$. Thus we obtain contrasting definitions of the value $\hat{\xi}$ for the cases of aiding and opposing flows, namely

$$\hat{\xi} = \begin{cases} 1-\mathrm{e}^{-1/(1+\lambda)} & \text{for } \lambda > 0 \\ 1-\mathrm{e}^{-1} & \text{for } \lambda < 0 \end{cases}. \tag{52}$$

The corresponding non-dimensional time, $\hat{\tau}$, at which the forward marching numerical scheme breaks down is

$$\hat{\tau} = \begin{cases} \dfrac{1}{1+\lambda} & \text{for } \lambda > 0 \\ 1 & \text{for } \lambda < 0 \end{cases}. \tag{53}$$

When the coefficient of $\partial^2 f/\partial\xi\partial\eta$ becomes negative in some region of the η-space, the problem is no longer well posed and the forward integration method breaks down.

The matching of the solution at $\xi = \xi^*$, equivalent to the time $\tau = \tau^*$, to the asymptotic steady state solution at $\xi = 1$ may now be achieved using a variation of the method first described by Dennis [21].

5.1. Numerical solution for $0 < \xi \leqslant \xi^*$

The evolution of the non-dimensional velocity function $\Phi(\xi,\eta) = \partial f/\partial\eta$ is governed by the integro-differential equation

$$\begin{aligned} &2\xi(1-\xi)[1+\ln(1-\xi)\Phi]\frac{\partial\Phi}{\partial\xi} \\ &\quad = \frac{\partial^2\Phi}{\partial\eta^2} + \frac{\partial\Phi}{\partial\eta}\left\{(1-\xi)\eta + [\xi+(1-\xi)\ln(1-\xi)]\right. \\ &\quad \left. \times \int_0^\eta \Phi(\xi,\eta')\,\mathrm{d}\eta' + 2\xi(1-\xi)\ln(1-\xi)\int_0^\eta \frac{\partial\Phi}{\partial\xi}(\xi,\eta')\,\mathrm{d}\eta'\right\} \end{aligned} \tag{54}$$

which has to be solved subject to the initial and boundary conditions

$$\Phi(0,\eta) = \mathscr{F}'(\eta), \quad \Phi(\xi,0) = 1+\lambda, \quad \Phi(\xi,\infty) = 1 \tag{55}$$

where the boundary condition $f(\xi,0) = 0$ has been incorporated in equation (54) and the steady state profile $\mathscr{F}'(\eta)$ is given in equation (18).

In order to proceed with a numerical analysis of equation (54), the η-space under investigation must first be restricted to finite dimensions. Therefore we regard $\eta = \eta_\infty$ to correspond to $\eta = \infty$ and divide this finite region into N equal grid spacings of length $h = \eta_\infty/N$. A variable ξ-step is used and the value of this step at the start of the j-th ξ increment is denoted by $\Delta\xi_j$. We also introduce the notation $\Phi_{i,j}$ to represent the finite-difference approximation to the non-dimensional velocity function Φ at the point $\eta = (i-1)h$ for some $\xi = \xi_j$, where h is a constant.

Given a complete solution $\Phi_{i,j}$, $i = 1,\ldots,N+1$, at $\xi = \xi_j$ we require the solution $\Phi_{i,j+1}$ at $\xi = \xi_{j+1} = \xi_j + \Delta\xi_j$ and adopt the step-by-step, finite-difference procedure described by Merkin [20]. This method is essentially an adaptation of the Crank–Nicolson approach and involves first approximating the ξ derivatives by central differences and the remaining terms by their averages over the j-th and $(j+1)$-th steps. Central differences are then introduced to estimate the spatial derivatives and the integrals in equation (54) are estimated using quadrature formulae following from the trapezium rule. Thus, the finite-difference equation

$$\begin{aligned} &S_{i+1,j+1/2} - 2S_{i,j+1/2} + S_{i-1,j+1/2} \\ &-4\chi_1(1-\chi_1)\frac{h^2}{\Delta\xi_j}\left(1+\frac{1}{2}\Lambda S_{i,j+1/2}\right)(S_{i,j+1/2} - 2\Phi_{i,j}) \\ &+\frac{1}{2}h^2(S_{i+1,j+1/2} - S_{i-1,j+1/2})\left[\left(\frac{1}{2}\chi_1 + (1-\chi_1)\chi_2\Lambda\right)\Omega_{i,j+1/2}\right. \\ &\left.+(i-1)(1-\chi_1) - 4\chi_1(1-\chi_1)\Lambda\frac{1}{\Delta\xi_j}\Theta_{i,j}\right] \end{aligned} \tag{56}$$

represents an approximation to the integro-differential equation (54) evaluated at $\eta = (i-1)h$ and $\xi = \xi_j + \frac{1}{2}\Delta\xi_j$, where

$$\begin{aligned} &S_{i,j+1/2} = \Phi_{i,j+1} + \Phi_{i,j}, \\ &\Omega_{i,j+1/2} = \frac{1}{2}(S_{1,j+1/2} + S_{i,j+1/2}) + \sum_{i'=2}^{i-1} S_{i',j+1/2} \\ &\chi_1 = \xi_j + \frac{1}{2}\Delta\xi_j, \quad \chi_2 = \frac{3}{2} + 2\frac{\xi_j}{\Delta\xi_j}, \\ &\Lambda = \ln(1-\chi_1), \quad \Theta_{i,j} = \frac{1}{2}(\Phi_{1,j} + \Phi_{i,j}) + \sum_{i'=2}^{i-1}\Phi_{i',j}, \end{aligned} \tag{57}$$

$2 \leqslant i \leqslant N$ and $j \geqslant 1$. The boundary conditions at $\eta = 0$ and $\eta = \infty$ further require that

$$S_{1,j+1/2} = 2(1+\lambda), \quad S_{N+1,j+1/2} = 2. \tag{58}$$

The system of nonlinear algebraic equations $G_i(S_{2,j+1/2},\ldots,S_{N,j+1/2}) = 0$, comprising equation (56) at $i = 2,\ldots,N$, thus defines a set of $(N-1)$ equations for $(N-1)$ unknowns. If $S^{(0)}_{i,j+1/2}$ is an approximation to the solution of this system, a better approximation for $S_{i,j+1/2}$ is defined by Newton's method and obtained by solving the resulting system of $(N-1)$ linear equations

$$\begin{aligned} &\sum_{i=2}^{N}(S_{i,j+1/2} - S^{(0)}_{i,j+1/2})\left(\frac{\partial G_k}{\partial S_{i,j+1/2}}\right)^{(0)} \\ &\qquad = -G_k(S^{(0)}_{2,j+1/2},\ldots,S^{(0)}_{N,j+1/2}), \quad k = 2,\ldots,N. \end{aligned} \tag{59}$$

To solve this linear system at each iteration we decompose the Jacobian matrix

$$\mathbf{J}_{ki} = \left(\frac{\partial G_k}{\partial S_{i,j+1/2}}\right)^{(0)}$$

into the product $\mathbf{J}=\mathbf{LU}$ of a lower-triangular matrix $\mathbf{L}$ and an upper-triangular matrix $\mathbf{U}$, using the method proposed by Doolittle and presented in Burden and Faires [22]. Thus the inversion of the linear system reduces to solving two systems involving the matrices $\mathbf{L}$ and $\mathbf{U}$ by direct and backward substitution, respectively. This iterative process is repeated until the absolute difference between successive approximations reaches a value less than some tolerance ε_1.

The forward integration commences at $\xi=0$ with the initial increment $\Delta\xi_0$, which is set to some prescribed small value, and a ξ-step doubling procedure is adopted. Given a complete solution at ξ_j and a previous step $\Delta\xi_{j-1}$ the solution at $\xi=\xi_j+2\Delta\xi_{j-1}$ is first calculated using the increment $2\Delta\xi_{j-1}$ and then using two separate increments of length $\Delta\xi_{j-1}$. If the absolute difference between the two solutions obtained at ξ_{j+1} is less than a preassigned tolerance ε_2 then the ξ-step is doubled so that $\Delta\xi_j=2\Delta\xi_{j-1}$. Otherwise the ξ increment remains unchanged.

5.2. Numerical solution for $\xi^*<\xi<1$

At $\xi=1$, corresponding to large values of the non-dimensional time τ, the solution for the non-dimensional velocity function $\Phi(\xi,\eta)=\partial f/\partial\eta$ is known to satisfy the ordinary differential equation (20) subject to the boundary conditions (21). This system defines the steady state configuration for which the profile $\Phi(1,\eta)=\mathscr{G}'(\eta)$ can be recovered numerically, using the techniques presented in Section 6.1, for a given buoyancy parameter λ.

The numerical solution described in Section 5.1 eventually breaks down at $\xi=\xi^*$ because the coefficient of $\partial\Phi/\partial\xi$ becomes small and is tending to negative values in part of the boundary-layer. The matching of the steady state solution at $\xi=1$ with that which is valid at $\xi=\xi^*$ is now achieved using an adaptation of the method of Dennis [21].

It is convenient to write the governing equation (12) in the form

$$\frac{\partial f}{\partial\eta}=\Phi \tag{60}$$

$$\frac{\partial^2\Phi}{\partial\eta^2}+p\frac{\partial\Phi}{\partial\eta}=q\frac{\partial\Phi}{\partial\xi} \tag{61}$$

where

$$p(\xi,\eta)=[\xi+(1-\xi)\ln(1-\xi)]f+(1-\xi)\eta+2\xi(1-\xi)\ln(1-\xi)\frac{\partial f}{\partial\xi}$$

$$q(\xi,\eta)=2\xi(1-\xi)[1+\ln(1-\xi)\Phi] \tag{62}$$

and $q(\xi,\eta)>0$ for all η when $\xi\leqslant\xi^*$.

The system of equations (60)–(62) must now be solved subject to the boundary conditions that the solution must coincide with that obtained by the step-by-step, forward integration method at $\xi=\xi^*$, and that at $\xi=1$ the solution is given by the steady state analysis. Thus the complete set of boundary conditions is given by

$$\begin{aligned}&\Phi(\xi^*,\eta)=\Phi^*(\eta),\quad \Phi(1,\eta)=\mathscr{G}'(\eta),\\ &f(1,\eta)=\mathscr{G}(\eta),\quad 0\leqslant\eta\leqslant\eta_\infty\\ &\Phi(\xi,0)=1+\lambda,\quad f(\xi,0)=0,\\ &\Phi(\xi,\eta_\infty)=1,\quad \xi^*\leqslant\xi\leqslant 1\end{aligned} \tag{63}$$

where the η-space under investigation has again been restricted to finite dimensions by regarding $\eta=\eta_\infty$ to correspond to $\eta=\infty$. A rectangular finite-difference grid with sides parallel to the η- and ξ-directions is constructed using n and m grid spaces and corresponding grid sizes $\tilde{h}=\eta_\infty/n$ and $\tilde{k}=1-\xi^*/m$, respectively.

A finite-difference approximation to equation (61) is now achieved by replacing the η-derivatives by central differences and the ξ-derivative $\partial\Phi/\partial\xi$ by either a backward or forward difference depending on whether $q(\xi,\eta)>0$ or $q(\xi,\eta)<0$, respectively. This formulation, using backward or forward differences, ensures that the matrix problem associated with our system of equations, along a line of constant ξ, remains diagonally dominant, in the sense described by Varga [23], and enables a convergent solution to be achieved using standard iterative techniques. Thus, equation (61) becomes

$$\left(1+\frac{1}{2}\tilde{h}p_{i,j}\right)\Phi_{i+1,j}+\left(1-\frac{1}{2}\tilde{h}p_{i,j}\right)\Phi_{i-1,j}-\left(2+\frac{\tilde{h}^2}{\tilde{k}}|q_{i,j}|\right)\Phi_{i,j}=\frac{\tilde{h}^2}{\tilde{k}}q_{i,j}\breve{\Phi}_{i,j} \tag{64}$$

for $2\leqslant i\leqslant n$ and $2\leqslant j\leqslant m$, where $\breve{\Phi}_{i,j}$ is defined by

$$\breve{\Phi}_{i,j}=\begin{cases}\Phi_{i,j+1} & \text{if } q_{i,j}<0\\ -\Phi_{i,j-1} & \text{if } q_{i,j}>0\end{cases} \tag{65}$$

and $\Phi_{i,j}=\Phi(\xi^*+(j-1)\tilde{k},\ (i-1)\tilde{h})$. Furthermore, the boundary conditions (63) require that

$$\begin{aligned}&\Phi_{i,1}=\Phi^*((i-1)\tilde{h}),\quad \Phi_{i,m+1}=\mathscr{G}'((i-1)\tilde{h}),\\ &f_{i,m+1}=\mathscr{G}((i-1)\tilde{h}),\quad 1\leqslant i\leqslant n+1\\ &\Phi_{1,j}=1+\lambda,\quad f_{1,j}=0,\\ &\Phi_{n+1,j}=1,\quad 1\leqslant j\leqslant m+1.\end{aligned} \tag{66}$$

To start the iterative scheme we must prescribe initial values of f and Φ throughout the solution domain. An approximation to the initial profile $f(\xi^*,\eta)$ is achieved by integrating equation (60) using the quadrature formulae following from the trapezium rule. Thus, at each j, $2\leqslant j\leqslant m$, we assume initial values for $f_{i,j}$, $2\leqslant i\leqslant n+1$, and $\Phi_{i,j}$, $2\leqslant i\leqslant n$, such that they follow a linear variation from the known solutions at $\xi=\xi^*$ and $\xi=1$. Initial approximations for the functions $p_{i,j}$ and $q_{i,j}$ follow from equation (62) by using a central-difference for the term $\partial f/\partial\xi$.

The iterative technique for solving the finite-difference system (64)–(66) now proceeds as follows:

(i) Fix the values of f, p and q throughout the domain and perform one complete sweep of the system (64)–(66) by the Gauss–Seidel method to calculate the new values of Φ. The grid points are swept along lines of constant ξ in the increasing η-direction, starting from $\xi = \xi^* + \tilde{k}$ and finishing at $\xi = 1 - \tilde{k}$. To increase the rate of convergence a successive over-relaxation procedure was employed with relaxation factor ω.

(ii) Integrate the differential equation (60) step-by-step along each line of constant ξ, using quadrature formulae based on the trapezium rule.

(iii) Using central differences to approximate the derivative $\partial f/\partial\xi$, values of p and q are re-calculated throughout the domain.

(iv) Continue to perform steps (i)–(iii) until convergence, i.e. until the average of the absolute difference in Φ over the domain between successive iterations falls below a prescribed tolerance ε_3.

6. Results

6.1. Numerical solution of the ordinary differential systems

The solution of both the ordinary differential equation (20), subject to the boundary conditions (21), which governs the solution behaviour for the final steady state at $\xi = 1$ at all values of λ, and the ordinary differential system (33), which governs the solution behaviour for the final steady state when $\lambda \gg 1$, can be achieved using the NAG routine D02HAF. This algorithm solves two-point boundary-value problems for systems of first-order, ordinary differential equations using a Runge–Kutta–Merson method and a Newton iteration in a shooting and matching technique. In this numerical procedure, an absolute error tolerance must be supplied and the upper range of integration must be specified at some finite value instead of infinity. In all the solutions of the system (20), (21) presented in this paper a tolerance of 10^{-8} and an endpoint of $\eta_\infty = 12$ were used as it was found that any further decrease and increase, respectively, of the values did not produce results which showed any further significant variation. However, for the solution of the system (33) it was necessary to advance the upper boundary to $\eta_\infty = 16$ to achieve the same conclusions.

The ordinary differential system (20), (21) was analysed by Merkin [19], wherein it was shown that solutions can only be achieved for $\lambda \geqslant \lambda_0$ and, furthermore, that the solution is only unique for $\lambda \geqslant -1$. The lower bound on λ is given by $\lambda_0 = -1.354108$ and the solutions for the non-dimensional skin friction coefficient at the plate surface $\mathscr{G}''(0)$, over a range of values of λ in the vicinity of $\lambda = 0$, are presented in Fig. 1(a). At $\lambda = -1$ the single solution is the well known Blasius solution. For $\lambda_0 < \lambda < -1$ two solutions exist, one continuing from the Blasius solution and the other such that $\mathscr{G}''(0) \to 0$ as $\lambda \to -1$, but this solution does not exist at $\lambda = -1$. Thus, we obtain a physically relevant solution only for $\lambda \geqslant -1$, i.e. the buoyancy parameter is such that the non-dimensional fluid velocity at the plate surface is never negative. Figure 1(a) also demonstrates that the expression (30) for $\mathscr{G}''(0)$ in the vicinity of $\lambda = 0$ provides an approximation to the non-dimensional skin friction coefficient which is graphically indistinguishable from the numerical solution over the range $|\lambda| \leqslant 0.35$.

The behaviour of the numerical solution of the system (20) and (21) for $\mathscr{G}''(0)$ at large values of λ is demonstrated in Fig. 1(b). The function (34), which approximates the non-dimensional skin friction coefficient in the case of pure free convection, follows by a numerical solution of the system (33) from which we find $\bar{\mathscr{G}}''(0) = -0.627555$. Thus, it can be seen in Fig. 1(b) that

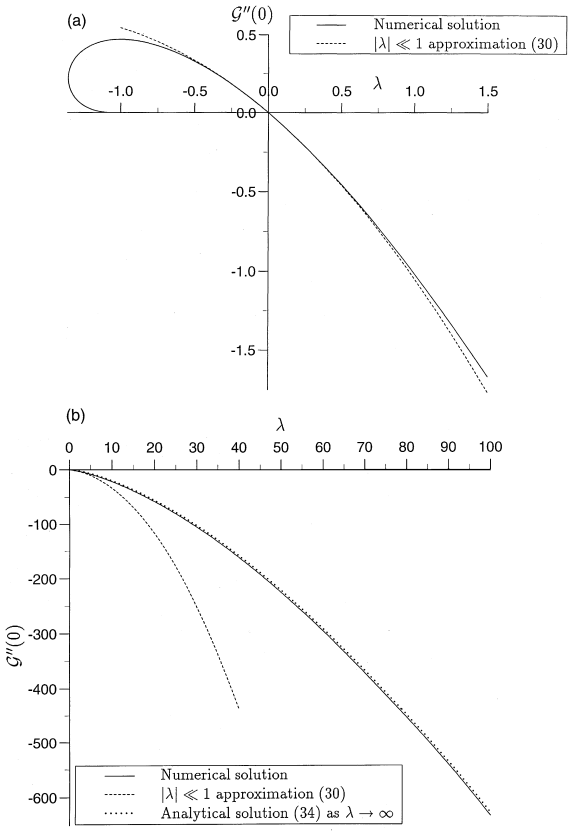

Fig. 1. The variation in the non-dimensional skin friction coefficient at the plate surface $\mathscr{G}''(0)$ for the final steady state with the buoyancy parameter λ. (a) In the vicinity of $\lambda = 0$ compared with the $|\lambda| \ll 1$ solution (30). (b) At large λ compared with the $\lambda \to \infty$ solution (34).

the function (34) provides an asymptote to which the non-dimensional skin friction coefficient tends as $\lambda \to \infty$.

Cheng [18] obtained the values of the ratio $Nu/Pe^{1/2}$ for pure free convection and pure forced convection numerically and, furthermore, subdivided the parameter space $\lambda \geqslant -1$ to provide us with the following approximate criteria for pure or mixed convection:

$-1 \leqslant \lambda < -0.15$, mixed flow

$-0.15 < \lambda < 0.15$, pure forced convection

$0.15 < \lambda < 16$, mixed flow

$16 < \lambda$, pure free convection. (67)

Examples of the profiles of the non-dimensional velocity function $\partial f/\partial\eta(1,\eta) = \mathscr{G}'(\eta)$ and the non-dimensional temperature function $\theta(1,\eta) = \lambda^{-1}(\mathscr{G}'(\eta)-1)$ over the range $\lambda \geqslant -1$ in the final steady state can be found in Cheng [18]. The corresponding initial unsteady profiles of the non-dimensional velocity $\mathscr{F}'(\eta)$ at $\xi = 0$ are presented in Fig. 2 whilst the initial unsteady temperature profile $\theta(0,\eta) = \mathrm{erfc}(\eta/\sqrt{2})$ is independent of λ. Thus, for the final steady state we have, (i) for $-1 \leqslant \lambda < 0$ the fluid velocity reduces as we approach the plate and is slower than the free stream flow U; (ii) at $\lambda = 0$ pure forced convection; (iii) for $\lambda > 0$ the non-dimensional boundary-layer thickness parameter can be shown to reduce as λ increases, since within the boundary-layer the fluid velocity is becoming increasingly greater than the free stream flow U; (iv) as $\lambda \to \infty$ pure free convection.

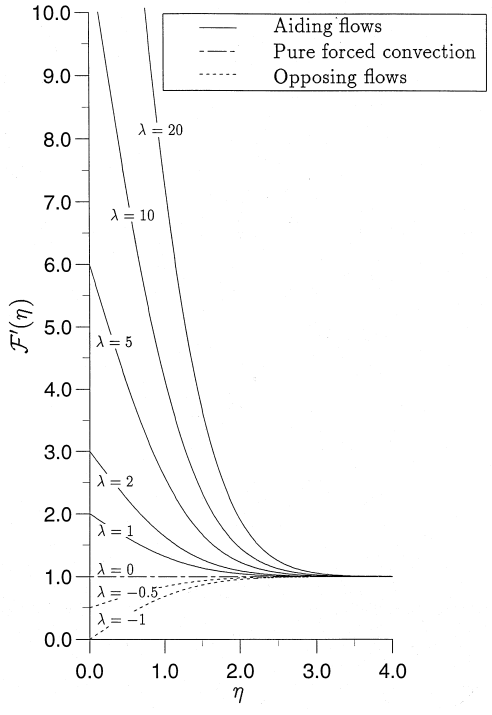

Fig. 2. The profiles of the non-dimensional velocity function $\mathscr{F}'(\eta)$ in the initial unsteady state for a range of buoyancy parameter values $\lambda \geqslant -1$.

The optimum values of the parameters introduced in Section 5.1 for the forward integration solution and Section 5.2 for the matching technique solution of the governing equation (12) are sought over a range of suitable values of the buoyancy parameter λ. We consider the cases $\lambda = -1.0$, -0.1, 0.1, 1.0 and 10.0 separately but discuss suitable values for these parameters mainly in terms of the case $\lambda = 0.1$.

6.2. Results for $0 < \xi \leqslant \xi^*$

The restriction to a finite dimensional η-space was achieved by taking $\eta_\infty = 12$. The effect on the forward integration numerical scheme of variations from this value of η_∞, whilst keeping h constant, was investigated and it was concluded that any larger value of η_∞ produced results which were indistinguishable from those presented in the figures. This observation is to be expected since the profiles $\mathscr{F}''(\eta)$, defining the initial unsteady state, and $\mathscr{G}''(\eta)$, defining the final steady state, over the complete range $\lambda \geqslant 1$ have all fallen below 10^{-9} at $\eta = 8$.

The values of the tolerances ε_1 and ε_2, as an average error over the $(N-1)$ unknown grid points, were taken to be $\varepsilon_1 = 10^{-7}$ and $\varepsilon_2 = 10^{-6}$, respectively. More restrictive values of both tolerances were considered and found to produce numerical results which did not show any significant variation. The observation that smaller values of ε_1 produce almost identical results follows from the fact that the iterative solution of the nonlinear system of algebraic equations (56) rapidly approaches a limiting value and satisfies the convergence criterion after only a few iterations.

The initial ξ increment was taken to be $\Delta\xi_0 = 10^{-7}$ in all the calculations presented in this paper. Any smaller initial ξ increment was soon increased after several steps by the doubling procedure described in Section 5.1 so that both the subsequent increments and the non-dimensional skin friction coefficient at corresponding instances were almost unchanged compared to those obtained using $\Delta\xi_0 = 10^{-7}$. For the buoyancy parameters $\lambda = -1.0$, -0.1, 0.1, 1.0 and 10.0, the ξ-step doubling criterion leads to final ξ increments of 1.024×10^{-4}, 8.192×10^{-4}, 8.192×10^{-4}, 1.024×10^{-4} and 6.4×10^{-6}, respectively.

The main source of variation in the solutions for the non-dimensional fluid velocity function $\partial f/\partial\eta(\xi,\eta)$ and skin friction coefficient $\partial^2 f/\partial\eta^2(\xi,0)$ arises by considering changes in the number of grid spaces N. It was observed that as N increases, and consequently h decreases, the initial development of the numerical solution approaches that of the small ξ solution. The values of N considered here were $N = 200$, 400, 800, 1600 and 3200 with corresponding values of $h = 0.06$, 0.03, 0.015, 0.0075 and 0.00375, respectively. A comparison of the values of the non-dimensional skin friction coefficient at the plate

surface, $\partial^2 f/\partial\eta^2(\xi,0)$, is presented in Table 1 for each value of N along with the small ξ solution (47) at various values of ξ, and corresponding τ, for the buoyancy parameter $\lambda = 0.1$. A similar comparison was carried out for other values of the buoyancy parameter λ and the solution for the skin friction coefficient was observed to be such that the function $-1/\lambda^{\partial^2 f/\partial\eta^2(\xi,0)}$ remained almost unchanged at the same value of ξ, as expected from the small ξ solution (47). The table illustrates that the numerical solutions, for different mesh sizes, vary most at small times when the finest grid produces the best approximation to the small ξ solution but for larger ξ, when the small ξ solution becomes invalid, the five solutions agree more closely. The value of ξ at which a further ξ increment would cause the forward integration method to break down is determined numerically to be approximately $\xi^* = 0.63201$, 0.63242, 0.59638, 0.39342 and 0.08689 for $\lambda = -1.0$, -0.1, 0.1, 1.0 and 10.0, respectively, which agree closely with the predicted values given in equation (52). The solution for $\Phi = \partial f/\partial\eta(\xi,\eta)$ is now continued using the method described in Section 5.2 which matches the velocity function profile $\Phi^*(\eta)$ at $\xi = \xi^*$, where the forward integration method described here terminates, to the steady state velocity function profiles $\mathscr{G}'(\eta)$ at $\xi = 1$, corresponding to $\tau = \infty$.

Figure 3 shows the variation of the non-dimensional velocity function $\partial f/\partial\eta(\xi,\eta)$ at various values of ξ, and corresponding times τ, for buoyancy parameters $\lambda = -1.0$ and 0.1, calculated using $h = 0.015$. The slight improvement in accuracy of the numerical solution as a whole is not felt to be justified for the additional computational time required by using smaller values of h. By plotting the initial unsteady profiles at $\xi = 0$, $\tau = 0$, given in equation (18), and the final steady state profiles at $\xi = 1$, $\tau \to \infty$, as predicted by the NAG routine solution of equation (20), the transition from $\tau = 0$ to $\tau = \infty$ is

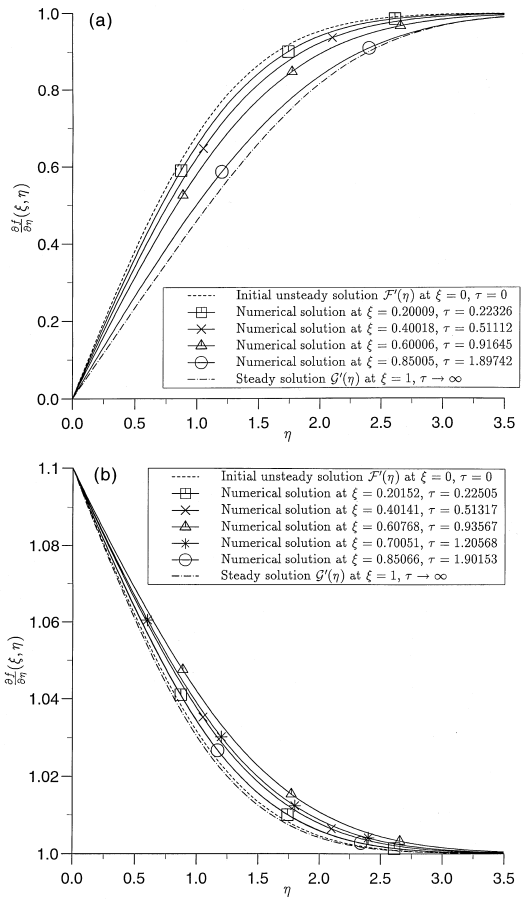

Fig. 3. Variation of the non-dimensional velocity function profile $\partial f/\partial\eta(\xi,\eta)$ as a function of η at various values of ξ and corresponding times τ during the evolution from the initial unsteady state (18) to the final steady state $\mathscr{G}'(\eta)$, derived from the solution of equation (20). (a) $\lambda = -1.0$, (b) $\lambda = 0.1$.

Table 1
Comparison of the small ξ solution (47), or the corresponding small time solution (49), with the forward integration solutions

ξ	Time τ	Numerical solution using N grid spacings					Small ξ or τ solution
		$N = 200$	$N = 400$	$N = 800$	$N = 1600$	$N = 3200$	
0.0005	0.00050	−0.0799038	−0.0798099	−0.0797863	−0.0797804	−0.0797790	−0.0797785
0.005	0.00501	−0.0798135	−0.0797199	−0.0796964	−0.0796905	−0.0796891	−0.0796886
0.05	0.05129	−0.0788973	−0.0788065	−0.0787837	−0.0787781	−0.0787766	−0.0787762
0.1	0.10536	−0.0778490	−0.0777615	−0.0777395	−0.0777341	−0.0777327	−0.0777324
0.2	0.22314	−0.0756454	−0.0755646	−0.0755443	−0.0755392	−0.0755380	−0.0755414
0.4	0.51083	−0.0706937	−0.0706270	−0.0706103	−0.0706061	−0.0706051	−0.0706793
0.59638	0.90727	−0.0647563	−0.0647059	−0.0646933	−0.0646902	−0.0646894	−0.0651621

Comparison is for the non-dimensional skin friction coefficient $\partial^2 f/\partial\eta^2(\xi,0)$ as predicted by different grid spacings in the numerical scheme for $\lambda = 0.1$.

clearly illustrated. In Fig. 3(a), when $\lambda = -1.0$, the choice of non-dimensional variables has the consequence of causing a uniform progression from the initial profile to the final steady state profile over all values of η rather than the initial development being focused on a small region of η-space. In Fig. 3(b), when $\lambda = 0.1$, rather than decreasing towards the final steady state profile, there is an increase in the fluid velocity function from the initial unsteady state over the whole η-space. The corresponding profiles of the non-dimensional temperature function $\theta(\xi, \eta)$ are not presented as they can be calculated from a simple transformation of the profiles of the fluid velocity function.

The behaviour of the non-dimensional skin friction coefficient $\partial^2 f/\partial \eta^2(\xi, 0)$ with ξ is illustrated in Fig. 4 for buoyancy parameters $\lambda = -1.0$ and 0.1. The transient numerical solution is shown to develop closely following the small ξ solution (47) and is graphically almost identical when $\xi \leqslant 0.35$ for $\lambda = -1.0$ and 0.1. In general, for $\lambda > 0$ the non-dimensional skin friction coefficient at the final steady state is less than the starting value at $\xi = 0$ but the numerical solution from the forward integration approach increases from $\xi = 0$ to a value at $\xi = \xi^*$, which is significantly higher than the value at $\xi = 1$. For $-1 \leqslant \lambda < 0$, the non-dimensional skin friction coefficient at the final steady state is again less than the starting value but the numerical solution from the forward integration approach now decreases with ξ.

In Fig. 5 we investigate the solution of the non-dimensional skin friction coefficient in terms of the more natural evolution variable τ. To allow a direct comparison of the variation in the solution with λ, the dependent variable being plotted is $-1/\lambda^{\partial^2 f/\partial \eta^2|_{\eta=0}}$ and hence, according to equation (19), all the evolutions must start at

$$-\frac{1}{\lambda}\frac{\partial^2 f}{\partial \eta^2}\bigg|_{\eta=0} = \sqrt{\frac{2}{\pi}}$$

at $\tau = 0$. For each of the buoyancy parameters $\lambda = -1.0$, -0.1, 0.1, 1.0 and 10.0, the λ-independent small time behaviour, defined using equation (49), clearly provides an accurate initial approximation. The fact that the forward integration solutions shown in Fig. 5 are almost identical was observed in the discussion of Table 1. At the indicated points $\tau = \tau^*$ the forward integrating, step-by-step method breaks down and we must complete the solution by attempting to match the final profile to the steady state profile at $\xi = 1$, where the function $-1/\lambda^{\partial^2 f/\partial \eta^2|_{\eta=0}}$ shows significant variation with λ.

The variation in the ratio $Nu/Pe^{1/2}$ with different buoy-

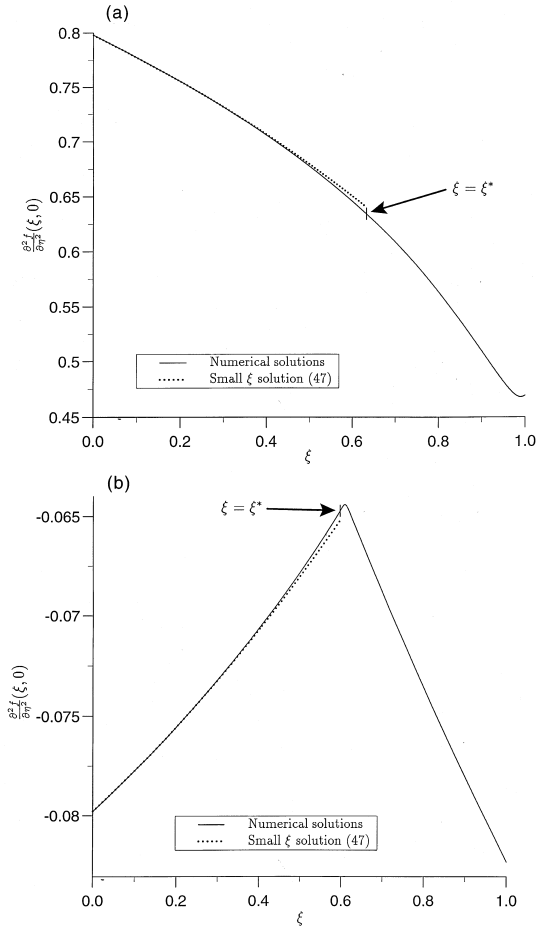

Fig. 4. The evolution of the non-dimensional skin friction coefficient at the plate surface $\partial^2 f/\partial \eta^2(\xi, 0)$ with ξ and the small ξ solution (47), where the transition from the solution method of Section 5.1 to that of Section 5.2 takes place at the indicated $\xi = \xi^*$. (a) $\lambda = -1.0$, (b) $\lambda = 0.1$.

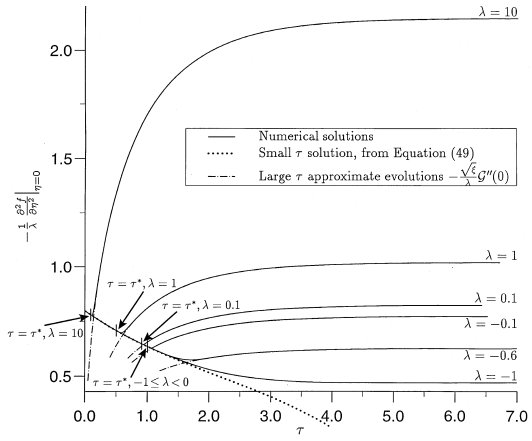

Fig. 5. The evolution of the function $-1/\lambda^{\partial^2 f/\partial \eta^2|_{\eta=0}}$ with time τ over a range of values of the buoyancy parameter $\lambda \geqslant -1$ and the small τ evolution derived from equation (49).

ancy parameters as time evolves is shown in Fig. 6. The initial evolution from the forward integration approach is in excellent agreement with the λ-independent small time solution (50).

6.3. Results for $\xi^* < \xi < 1$

The transition from the non-dimensional velocity function profile $\Phi^*(\eta) = \partial f/\partial\eta(\xi^*, \eta)$ to the steady state solution at $\xi = 1$ is, in general, quite non-trivial. Indeed the whole of the profiles for the parameter values $\lambda > 0$, as shown in Fig. 3(b) for $\lambda = 0.1$, have reached values at $\xi = \xi^*$ which are further from the final steady state values than they were originally at $\xi = 0$. The profiles for $-1 \leqslant \lambda < 0$ display a slightly different behaviour, but we will see that again the matching of the profile at $\xi = \xi^*$ to that at $\xi = 1$ is indirect. The transients presented here beyond the time at which the forward integration approach breaks down are in contrast to the results for some similar problems, see for example Harris et al. [13, 14], where the two profiles to be matched are relatively similar. Satisfactory results for a suddenly heated vertical plate have been obtained by Ingham and Brown [10], but when the plate is placed in a non-porous medium, the coupled differential equations cannot be solved by means of a smooth transition to the final steady state solution, see Ingham [24, 25].

The restriction of the solution domain to finite dimensions is achieved by retaining the value $\eta_\infty = 12$ and the convergence criterion was set by assigning the value $\varepsilon_3 = 10^{-13}$ for the tolerance. This value produces a numerical solution in which the peak value of the skin friction coefficient for $\lambda = 0.1$ is thought to be accurate to about seven significant figures for a particular set of parameters under investigation and had to be made small due to the slow rate of convergence of this method. The use of the relaxation parameter ω was successful in increasing the rate of convergence. The optimum value was found to be the largest value for which the numerical scheme converged and this was found to be around $1.2 \leqslant \omega \leqslant 1.4$, depending upon the buoyancy parameter being used.

Transient numerical solutions for the non-dimensional velocity function $\Phi = \partial f/\partial\eta(\xi, \eta)$ were found using spatial mesh widths of $\tilde{h} = 0.06$, 0.03, 0.015 and 0.0075, where the initial profile $\Phi^*(\eta)$ was taken to be the profile obtained using the appropriate number of mesh points N in the forward integration approach. For the buoyancy parameter $\lambda = 0.1$, a variety of mesh sizes $\tilde{k}$ in the ξ-direction were used for each of these four spatial meshes to determine the evolution of the skin friction coefficient over the interval $\xi^* < \xi < 1$. As the spatial mesh was refined from $n = 200$ to $n = 400$, a significant difference in this evolution was observed, especially in the vicinity of the local maximum, but the variation with further refinements to $n = 800$ and $n = 1600$ was not so large. The computational effort required to proceed to a spatial grid with $n = 1600$ was therefore not felt to be justified. The variation in the solution beyond $\xi = \xi^*$ and within the vicinity of the local maximum for $\lambda = 0.1$ is represented graphically in Fig. 7 where the contrast between different mesh widths $\tilde{k}$ using the three different spatial grids $n = 400$, $n = 800$ and $n = 1600$ can be clearly seen. The small area of $(\xi, \partial^2 f/\partial\eta^2(\xi, \eta))$ space depicted in Fig. 7 encompasses the region in which the most significant effect of variations in mesh widths $\tilde{h}$ and $\tilde{k}$ are observed. In the cases $n = 400$ and $n = 800$, as we refine the ξ mesh over the range $m = 300$ to $m = 800$ grid spaces a limiting numerical solution is approached. This conclusion should be expected from the final ξ increment reached in the

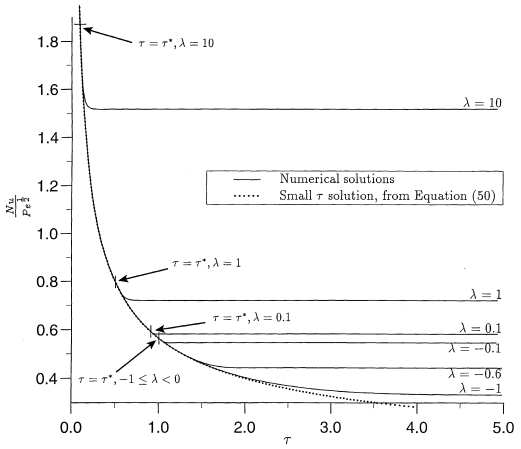

Fig. 6. The evolution of the ratio $Nu/Pe^{1/2}$ with time τ over a range of values of the buoyancy parameter $\lambda \geqslant -1$ and the small τ evolution derived from equation (50).

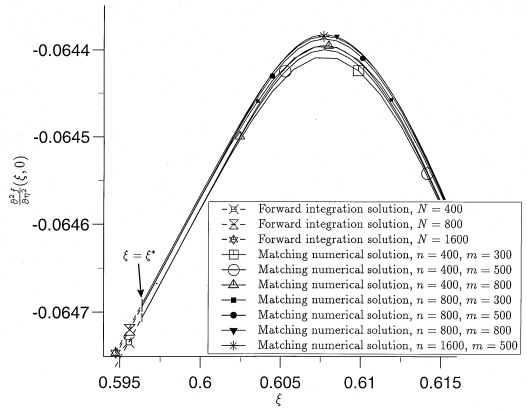

Fig. 7. A comparison of the matching method solutions achieved in the vicinity of the local maximum of the non-dimensional skin friction coefficient at the plate surface using different mesh sizes in the ξ and η directions and the buoyancy parameter $\lambda = 0.1$.

forward integration scheme which predicts that approximately $m = 493$ mesh spaces are required to maintain the same ξ-step. Thus, at such values of $\tilde{k}$, the transition from the forward integration method to the matching method is represented by a smooth skin friction coefficient evolution at $\xi = \xi^*$. A single solution is presented using an $n = 1600$ spatial grid, with $m = 500$, to demonstrate the minimal variation with spatial grid refinements beyond $n = 800$.

A numerical solution, using the matching method presented in Section 5.2, was also performed for the case $\lambda = 0.1$ using the variable τ, rather than ξ, and imposing the steady state solution to apply at some large, but finite, time $\tau = \tau_\infty$. Reasonable agreement between the two approaches was found at the same spatial mesh sizes. However, to reach a comparable number of grid points around the local maximum of the skin friction coefficient solution would require a vast number of τ mesh points. Thus, the matching method in terms of the ξ variable has a distinct advantage over the matching method using τ in that, when transformed back to the more natural time evolution, the mesh in terms of ξ naturally provides a higher concentration of mesh points at smaller values of τ, where the solution is changing most rapidly, but a lower concentration at later times when the solution is asymptoting towards the steady state value.

As a further check on the accuracy of the matching method approach, the step-by-step method was terminated at a ξ-value before $\xi = \xi^*$ and in the case of $\lambda = 0.1$ we ceased integration at the value $\xi = 0.5$. The matching method was then applied over this larger ξ interval and compared against a solution achieved over $\xi^* < \xi < 1$ using a comparable value of $\tilde{k}$. The evolution of the non-dimensional skin friction coefficient was found to be very similar and in particular the same behaviour around the local maximum was observed.

A spatial grid in which $n = 800$ and $h = 0.015$ was used for all the solutions from the matching method presented in Figs 3–6. It was observed in the discussion of Fig. 7 that a smooth transition from the forward integration approach to the matching method is achieved if we attempt to continue the ξ increment in use at $\xi = \xi^*$ over to $\xi > \xi^*$. The solutions presented for $\lambda = -1.0$, -0.1, 0.1, 1.0 and 10.0 have been calculated using $m = 800$, 500, 500, 1000 and 1000, respectively, and therefore we have only been able to retain the same ξ increment in the cases $\lambda = \pm 0.1$. Clearly, computational capabilities limit the amount of refinement that can be carried out on the ξ-grid in this matching method. Despite this loss of accuracy, the transition from the forward integration method to the matching method at $\xi = \xi^*$ is still seen to be smooth in Figs 5 and 6.

Further profiles of the non-dimensional velocity function $\partial f/\partial\eta(\xi, \eta)$, which were achieved using the matching method beyond $\xi = \xi^*$ for buoyancy parameters $\lambda = -1.0$ and 0.1, are included in Fig. 3. In Fig. 3(a), the uniform progression from the initial profile to the final steady state profile over all values of η continues until approximately $\xi = 0.98$ when the solution slightly overshoots the final steady state profile. Thus, the profile at $\xi = 1$ is approached as $\tau \to \infty$ from smaller velocity function values. In Fig. 3(b), soon after $\xi = \xi^*$, and more precisely at $\xi \approx 0.60768$, a peak value of the solution profile is achieved over all values of η. The velocity function profile subsequently decreases monotonically past the initial profile and progresses uniformly in η-space to the steady state profile valid at $\xi = 1$, or $\tau \to \infty$. The regularity of the variation in the solution profile over the whole η-space is emphasized by comparing the velocity functions at $\xi = 0.20152$ and $\xi = 0.85066$ in Fig. 3(b) which are indistinguishable at graphical resolution over all values of η.

The complete behaviour of the non-dimensional skin friction coefficient with ξ, shown in Fig. 4 for buoyancy parameters $\lambda = -1.0$ and 0.1, can now be realized. As described for the velocity function profiles in Fig. 3, for $\lambda = -1.0$ we obtain an almost monotonic decrease in $\partial^2 f/\partial\eta^2(\xi, 0)$ with a small local minimum just before $\xi = 1$. When transformed to an evolution with respect to τ, this apparently significant minimum becomes graphically negligible as it takes place over a large time interval. Figure 4(b) depicts the development of the skin friction coefficient for $\lambda = 0.1$ and the relatively sharp local maximum observed, before a steady monotonic decrease with ξ towards the steady state value.

The evolutions of the function $-1/\lambda^{\partial^2 f/\partial\eta^2_{|\eta=0}}$ with time at different values of the buoyancy parameter λ, shown in Fig. 5, demonstrate how the solutions for $\lambda > -1$ all move away fairly rapidly from the curve given by the solution at $\lambda = -1$ and pass through a minimum point after the forward integration approach breaks down. For $\lambda > 0$, both the time of deviation and the time $\tau = \tau^*$ reduce as we increase λ. Thus, if λ is large the initial interval over which the $\lambda = -1$ solution curve is traced becomes small and the evolution rapidly approaches the large steady state asymptotic value as we approach pure free convection. For $-1 < \lambda < 0$, a further solution at $\lambda = -0.6$, using $m = 800$, has been added to establish the dependence on the buoyancy parameter. As λ approaches -1 within this interval, the time at which the local minimum is achieved and the time interval over which the $\lambda = -1$ solution is traced both increase whilst the forward integration approach still breaks down at $\tau^* \approx 1$, as predicted by equation (53). The local minimum also becomes smoother as $\lambda \to -1$ so that it becomes almost graphically imperceptible at $\lambda = -1$. The evolution for $\lambda = -1$ thus represents a lower limiting solution for the function $-1/\lambda^{\partial^2 f/\partial\eta^2_{|\eta=0}}$.

The profile of the ratio $Nu/Pe^{1/2}$ at $\lambda = -1$, shown in Fig. 6, again provides a limiting lower bound for the solution at $\lambda > -1$. At a given value of λ, the solution for this ratio approximately traces the $\lambda = -1$ evolution

before breaking away abruptly and reaching values close to the final steady state ratio over a very short time interval. This almost constant behaviour of the ratio $Nu/Pe^{1/2}$ after deviation from the $\lambda = -1$ solution suggests that the evolution of the function shown in Fig. 5 at such times can be accurately approximated by the function $-(\sqrt{\xi}/\lambda)\,\mathscr{G}''(0)$ for $\lambda > -1$. To emphasize this point these approximations have been superimposed onto Fig. 5.

A solution of the governing system (12) and (13) in the special case $\lambda = 0$, when the surface temperature remains unchanged, can be obtained as $f(\xi,\eta) = \eta$ and $\theta(\xi,\eta) = 1$, from equation (6). Thus, the evolutions plotted in Figs 5 and 6 apparently become indeterminate for $\lambda = 0$. However, the behaviour of the function $-1/\lambda^{\partial^2 f/\partial\eta^2_{|\eta=0}}$ and the ratio $Nu/Pe^{1/2}$ at $\lambda = 0$ can be achieved by a limiting process from the known small ξ approximations, which are independent of λ, and the solutions at $\xi = 1$. The evolutions in Figs 5 and 6 for the case of pure forced convection can therefore be expected to initially trace along the $\lambda = -1$ curve, deviating from this curve at some point between the points of deviation of the $\lambda = \pm 0.1$ curves. The asymptotes for the curves are then the value $\sqrt{2/\pi}$ for Fig. 5, i.e. a return to the value at $\xi = 0$, and $1/\sqrt{\pi}$ for Fig. 6. The limiting process can be achieved by constraining the curves in Figs 5 and 6 for pure forced convection to lie between all pairs of $\lambda = \pm\varepsilon$ solutions as $\varepsilon \to 0$.

7. Conclusions

Unsteady mixed convection from a vertical plate embedded in a fluid-saturated porous medium, which occurs as the temperature on the surface is instantaneously changed from the ambient temperature T_∞ to a constant temperature T_w and is driven by a uniform free stream flow, has been analyzed in detail. Transient numerical solutions of the governing equations have been presented over the range of physically relevant buoyancy parameter values, $\lambda \geqslant -1$, which model the cases in which the buoyancy forces are both aiding and opposing the free stream.

From an analytical investigation of the governing boundary-layer equations we have been able to deduce solutions for the non-dimensional velocity function, the skin friction coefficient and the ratio $Nu/Pe^{1/2}$ in the initial unsteady state, at small times and for the final steady state. The numerical solutions of the full boundary-layer equations were found to both approach limiting evolutions as the mesh sizes were refined and agree excellently with the small time solutions, thus ensuring the validity of the numerical approaches.

The most innovative result that has been observed in this application of a standard forward integration and matching approach to the solution of the governing parabolic equation lies in the fact that accurate solutions have been achieved in the second method despite the indirect nature of their evolutions. The profiles of the fluid velocity function at the time when the step-by-step method breaks down are often found to be further from the known steady state profiles than they were in the original unsteady state. Nevertheless, for the complete range of buoyancy parameters considered, a matching solution could still be achieved, using the method of Dennis [21], and significantly different initial and final profiles, which approached a limiting evolution with grid refinement. A considerable advantage was found with the use of a transformed, finite time scale in which $\tau = \infty$ corresponds to $\xi = 1$. This enabled a higher concentration of grid points to be used at smaller times near the turning point of the skin friction coefficient as a function of ξ and thus a smooth transition from the forward integration approach to the matching approach could be achieved. Similar problems have been attempted in non-porous media, see Ingham [24, 25], but the governing coupled parabolic equations cannot be solved by means of smooth transitions, such as those displayed in this paper, to the final steady state solution.

References

[1] D.A. Nield, A. Bejan, Convection in Porous Media, Springer, Berlin, 1992.
[2] M. Kaviany, Principles of Heat Transfer in Porous Media, Springer, New York, 1991.
[3] A. Nakayama, PC-Aided Numerical Heat Transfer and Convective Flow, CRC Press, Tokyo, 1995.
[4] D.B. Ingham, I. Pop. (Eds.), Transport Phenomena in Porous Media, Elsevier, Oxford, 1997 (in press).
[5] C.H. Johnson, P. Cheng, Possible similarity solutions for free convection boundary layers adjacent to flat plates in porous media, International Journal of Heat and Mass Transfer 21 (1978) 709–718.
[6] D.B. Ingham, J.H. Merkin, I. Pop, Flow past a suddenly cooled vertical flat surface in a saturated porous medium, International Journal of Heat and Mass Transfer 25 (1982) 1916–1919.
[7] D.B. Ingham, J.H. Merkin, I. Pop, Flow past a suddenly cooled horizontal flat surface in a saturated porous medium, Acta Mechanica 56 (1985) 205–217.
[8] I. Pop, P. Cheng, The growth of a thermal layer in a porous medium adjacent to a suddenly heated semi-infinite horizontal surface, International Journal of Heat and Mass Transfer 26 (1983) 1574–1576.
[9] P. Cheng, I. Pop, Transient free convection about a vertical flat plate embedded in a porous medium, International Journal of Engineering Science 22 (1984) 253–264.
[10] D.B. Ingham, S.N. Brown, Flow past a suddenly heated vertical plate in porous media, Proceedings of the Royal Society London, Ser. A 403 (1986) 51–80.
[11] J.H. Merkin, G. Zhang, The boundary-layer flow past a

suddenly heated vertical surface in a saturated porous medium, Wärme- und Stoffübertragung 27 (1992) 299–304.
[12] S.D. Harris, D.B. Ingham, I. Pop, Transient free convection on a vertical plate subjected to a change in surface heat flux in porous media, Fluid Dynamics Research 18 (1996) 313–324.
[13] S.D. Harris, D.B. Ingham, I. Pop, Free convection from a vertical plate in a porous medium subjected to a sudden change in surface heat flux, Transport in Porous Media 26 (1997) 207–226.
[14] S.D. Harris, D.B. Ingham, I. Pop, Free convection from a vertical plate in a porous media subjected to a sudden change in surface temperature, International Communications in Heat and Mass Transfer 24 (1997) 543–552.
[15] S.H. Smith, The impulsive motion of a wedge in a viscous fluid, Journal of Applied Mathematics and Physics (ZAMP) 18 (1967) 508–522.
[16] S. Bhattacharyya, A. Pal, N. Datta, Flow and heat transfer due to impulsive motion of a cone in a viscous fluid, Heat and Mass Transfer 30 (1995) 303–307.
[17] M. Kumari, G. Nath, Boundary layer development on a continuous moving surface with a parallel free stream due to impulsive motion, Heat and Mass Transfer 31 (1996) 283–289.
[18] P. Cheng, Combined free and forced convection flow about inclined surfaces in porous media, International Journal of Heat and Mass Transfer 20 (1977) 807–813.
[19] J.H. Merkin, Mixed convection boundary layer flow on a vertical surface in a saturated porous medium, Journal of Engineering Mathematics 14 (1980) 301–313.
[20] J.H. Merkin, Free convection with blowing and suction, International Journal of Heat and Mass Transfer 15 (1972) 989–999.
[21] S.C.R. Dennis, The motion of a viscous fluid past an impulsively started semi-infinite flat plate, Journal of the Institute of Mathematics and its Applications 10 (1972) 105–117.
[22] R.L. Burden, J.D. Faires, Numerical Analysis, 5th ed., PWS, Boston, 1993.
[23] R.S. Varga, Matrix Iterative Analysis, Prentice-Hall, Englewood Cliffs, NJ, 1962.
[24] D.B. Ingham, Transient free convection on an isothermal vertical flat plate, International Journal of Heat and Mass Transfer 21 (1978) 67–69.
[25] D.B. Ingham, Numerical results for flow past a suddenly heated vertical plate, Physics of Fluids 21 (1978) 1891–1895.